Astronomy & Astrophysics

First AGILE catalog of high-confidence gamma-ray sources

C. Pittori[1], F. Verrecchia[1], A. W. Chen[2,3], A. Bulgarelli[4], A. Pellizzoni[5], A. Giuliani[2,3], S. Vercellone[6], F. Longo[7,8], M. Tavani[9,10,11,3], P. Giommi[1,12], G. Barbiellini[7,8,3], M. Trifoglio[4], F. Gianotti[4], A. Argan[9], A. Antonelli[13], F. Boffelli[14], P. Caraveo[2], P. W. Cattaneo[14], V. Cocco[10], S. Colafrancesco[1,12], T. Contessi[2], E. Costa[9], S. Cutini[1], F. D'Ammando[9,10], E. Del Monte[9], G. De Paris[9], G. Di Cocco[4], G. Di Persio[9], I. Donnarumma[9], Y. Evangelista[9], G. Fanari[1], M. Feroci[9], A. Ferrari[3,15], M. Fiorini[2], F. Fornari[2], F. Fuschino[4], T. Froysland[3,11], M. Frutti[9], M. Galli[16], D. Gasparrini[1], C. Labanti[4], I. Lapshov[9,17], F. Lazzarotto[9], F. Liello[9], P. Lipari[18,19], E. Mattaini[2], M. Marisaldi[4], M. Mastropietro[9,21], A. Mauri[4], F. Mauri[14], S. Mereghetti[2], E. Morelli[4], E. Moretti[7,8], A. Morselli[11], L. Pacciani[9], F. Perotti[2], G. Piano[9,10,11], P. Picozza[10,11], M. Pilia[22,2,5], C. Pontoni[3,8], G. Porrovecchio[9], B. Preger[1], M. Prest[8,22], R. Primavera[1], G. Pucella[9], M. Rapisarda[20], A. Rappoldi[14], E. Rossi[4], A. Rubini[9], S. Sabatini[10], P. Santolamazza[1], E. Scalise[9], P. Soffitta[9], S. Stellato[1], E. Striani[10], F. Tamburelli[1], A. Traci[4], A. Trois[9], E. Vallazza[8], V. Vittorini[9,3], A. Zambra[2,3], D. Zanello[18,19], and L. Salotti[12]

[1] ASI Science Data Center, ESRIN, 00044 Frascati (RM), Italy
    e-mail: pittori@asdc.asi.it
[2] INAF-IASF Milano, via E. Bassini 15, 20133 Milano, Italy
[3] Consorzio Interuniversitario Fisica Spaziale (CIFS), villa Gualino - v.le Settimio Severo 63, 10133 Torino, Italy
[4] INAF-IASF Bologna, via Gobetti 101, 40129 Bologna, Italy
[5] Osservatorio Astronomico di Cagliari, loc. Poggio dei Pini, strada 54, 09012, Capoterra (CA), Italy
[6] INAF-IASF Palermo, via Ugo La Malfa 153, 90146 Palermo, Italy
[7] Dip. Fisica, Università di Trieste, via A. Valerio 2, 34127 Trieste, Italy
[8] INFN Trieste, Padriciano 99, 34012 Trieste, Italy
[9] INAF-IASF Roma, via del Fosso del Cavaliere 100, 00133 Roma, Italy
[10] Dipartimento di Fisica, Università Tor Vergata, via della Ricerca Scientifica 1, 00133 Roma, Italy
[11] INFN Roma Tor Vergata, via della Ricerca Scientifica 1, 00133 Roma, Italy
[12] Agenzia Spaziale Italiana, viale Liegi 26, 00198 Roma, Italy
[13] Osservatorio Astronomico di Roma, via di Frascati 33, 00040 Monte Porzio Catone, Italy
[14] INFN Pavia, via Bassi 6, 27100 Pavia, Italy
[15] Dipartimento di Fisica, Università di Torino, via P. Giuria 15, 10126 Torino, Italy
[16] ENEA Bologna, via don Fiammelli 2, 40128 Bologna, Italy
[17] IKI, Moscow, Russia
[18] INFN Roma 1, p.le Aldo Moro 2, 00185 Roma, Italy
[19] Dip. Fisica, Università La Sapienza, p.le Aldo Moro 2, 00185 Roma, Italy
[20] ENEA Frascati, via Enrico Fermi 45, 00044 Frascati (RM), Italy
[21] CNR, IMIP, Area Ricerca Montelibretti (RM), Italy
[22] Dip. Fisica, Università dell'Insubria, via Valleggio 11, 22100 Como, Italy

ABSTRACT

We present the first catalog of high-confidence γ-ray sources detected by the AGILE satellite during observations performed from July 9, 2007 to June 30, 2008. Cataloged sources were detected by merging all the available data over the entire time period. AGILE, launched in April 2007, is an ASI mission devoted to γ-ray observations in the 30 MeV–50 GeV energy range, with simultaneous X-ray imaging capability in the 18–60 keV band. This catalog is based on Gamma-Ray Imaging Detector (GRID) data for energies greater than 100 MeV. For the first AGILE catalog, we adopted a conservative analysis, with a high-quality event filter optimized to select γ-ray events within the central zone of the instrument field of view (radius of 40°). This is a significance-limited (4σ) catalog, and it is not a complete flux-limited sample due to the non-uniform first-year AGILE sky coverage. The catalog includes 47 sources, 21 of which are associated with confirmed or candidate pulsars, 13 with blazars (7 FSRQ, 4 BL Lacs, 2 unknown type), 2 with HMXRBs, 2 with SNRs, 1 with a colliding-wind binary system, and 8 with unidentified sources.

Key words. gamma rays: observations – catalogs

1. Introduction

AGILE (Astrorivelatore Gamma ad Immagini LEggero) (Tavani et al. 2008, 2009a) is a mission of the Italian Space Agency (ASI) devoted to γ-ray astrophysics in the 30 MeV–50 GeV and

18–60 keV energy ranges. AGILE was successfully launched on April 23, 2007 in a ~550 km equatorial orbit with low inclination angle, ~2.5°. High-energy γ-ray astrophysics is entering a new challenging phase of discovery. During the 1970's and 1980's, the SAS-2 (Fichtel et al. 1975) and COS-B
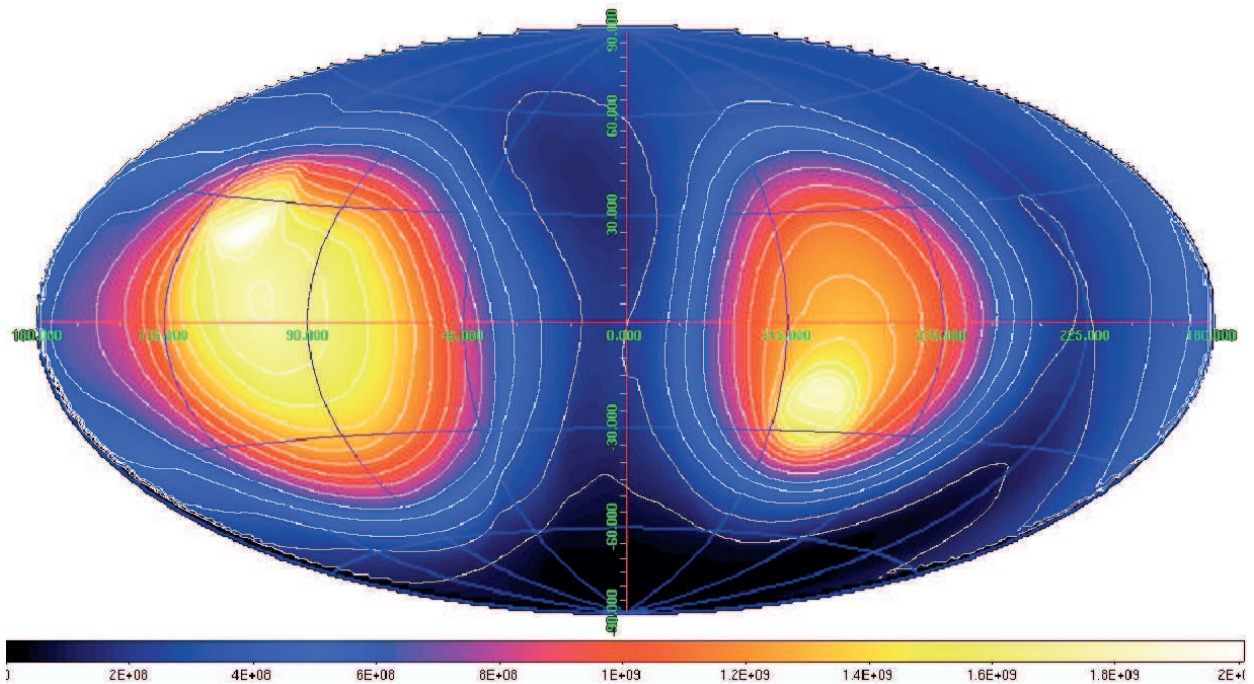
Fig. 1. Total AGILE-GRID exposure sky map in Aitoff projection and Galactic coordinates, for energies >100 MeV in units of cm² s, accumulated during the period July 9, 2007–June 30, 2008 (with the F4 event filter). The regions of deeper exposures (whiter in the color scale) are a consequence of the AGILE specific pointings at the Galactic plane, combined with the effect of Earth occultation.

(Bignami et al. 1975; Bennet et al. 1977) space missions discovered the very first cosmic γ-ray sources around 100 MeV, but our knowledge of high-energy cosmic γ-ray emission and phenomena up to now was mainly based on the remarkable results obtained by the EGRET instrument, onboard the Compton Gamma-Ray Observatory (CGRO) (Thompson et al. 1993). Nearly 300 γ-ray sources above 100 MeV were detected by EGRET (Hartman et al. 1999) during the period from April 22, 1991 to October 3, 1995; however, only a small fraction of them (~30%) have currently been identified. Many sources are variable or transient on short timescales, and our understanding of many high energy phenomena is still preliminary.

AGILE is the first γ-ray mission operating in space after almost ten years since the end of EGRET operations. AGILE was the only mission entirely dedicated to high-energy astrophysics above 30 MeV during the period April 2007–June 2008. It is currently operating together with the Fermi Gamma-Ray Space Telescope (formerly GLAST), launched on June 11, 2008 (Michelson 2008; Atwood et al. 2009). The highly innovative AGILE instrument is the first of a new generation of high-energy space missions based on solid-state silicon technology, expected to substantially advance our knowledge in several research areas including the study of active galactic nuclei, gamma-ray bursts, pulsars, unidentified γ-ray sources, Galactic compact objects, supernova remnants, etc.

The AGILE Payload detector consists of the silicon tracker (ST) (Barbiellini et al. 2001; Prest et al. 2003), the X-ray detector SuperAGILE (Feroci et al. 2007), the CsI(Tl) Mini-Calorimeter (MCAL) (Labanti et al. 2006), and an anticoincidence system (ACS) (Perotti et al. 2006). The combination of ST, MCAL, and ACS forms the Gamma-Ray Imaging Detector (GRID). Accurate timing, positional and attitude information is provided by the precise positioning system and the two star sensors units. The silicon tracker, based on the process of photon conversion into electron-positron pairs, is the core of the AGILE-GRID. It

consists of a total of 12 trays, the first 10 of which are capable of converting γ-rays by a Tungsten layer tracked by silicon microstrip detectors providing the two orthogonal coordinates for each element (point) along the track. AGILE-GRID event processing is operated by onboard trigger logic algorithms (Argan et al. 2004) and by on-ground event filtering. In this paper we use the on-ground GRID event filter called "F4" (Giuliani et al. 2006).

During its first year in orbit, AGILE surveyed the γ-ray sky and detected many galactic and extragalactic sources. The AGILE Commissioning phase ended on July 9, 2007, and the following science verification phase lasted about four months, up to November 30, 2007. On December 1, 2007 the baseline nominal observations and pointing plan of Cycle-1 started with the guest observer program. In this paper we present the first catalog of high-confidence γ-ray sources detected by AGILE including data from July 9, 2007 to June 30, 2008, thus covering science verification phase data and the first seven months of the Cycle-1. Cataloged sources are detected by merging all the available data over the entire time period.

This is a significance-limited catalog that includes only sources above 4σ extracted from the sample of AGILE detections obtained with a conservative data analysis, as described in the following sections. The catalog sensitivity is nonuniform, reflecting the inhomogeneous first-year AGILE sky coverage. The first-year exposure (see Fig. 1) was focused mainly towards the Galactic plane, mostly in the Carina-Crux and in the Cygnus regions. The average effective AGILE-GRID exposure time across the sky, for the chosen F4 event filter, is $\langle T_{exp} \rangle \simeq 0.8 \times 10^6$ s, with peak values of $\sim 7 \times 10^6$ s. For a given statistical significance, the limiting point-source flux varies with position, owing to the diffuse γ-ray emission that represents a nonuniform background over which the pointlike sources are seen. The Galactic diffuse continuum γ-ray emission dominates other components and has a wide distribution with most emission coming from the Galactic

plane. We detect limiting fluxes of about 2×10^{-7} ph cm^{-2} s^{-1} with $\sim 4\sigma$ statistical significance at galactic latitudes $|b| > 10°$.

The outline of the paper is as follows. In Sect. 2 we briefly discuss the AGILE-GRID response characteristics and in Sect. 3 describe the AGILE diffuse γ-ray model used in the data analysis. In Sect. 4 we describe the satellite pointing strategy and data flow. We then present in Sect. 5 the data reduction and analysis method used to build the first AGILE catalog. Our results and the list of detected high-confidence γ-ray sources are shown in Sect. 6. Finally in Sect. 7 we discuss our results and make some concluding remarks.

2. AGILE-GRID response characteristics

The AGILE-GRID inflight calibration during the first year and a half of observations has been recently completed and details of the instrument response characteristics will be given in Tavani et al. (2009b). The results are consistent with prelaunch simulations and instrument tests (Tavani et al. 2009a).

The energy-dependent in-flight GRID instrument point spread function (PSF) has a full-width at half-maximum (*FWHM*) of approximately 3.5° at 100 MeV, and gradually improves at higher energies. AGILE PSF is better than that of EGRET by a factor of ~2 above 400 MeV. The GRID effective area, as determined by inflight calibrations, reaches 500 cm^2 at several hundred MeV, depending on the GRID event filter used. The conservative event filter F4, chosen for our analysis, applies tight event selection cuts to eliminate a higher fraction of possible particle background counts. This filter is optimized to select γ-ray events within the central field of view (FoV) zone (~40° radius) at the expense of the effective area. In the energy range 200–400 MeV and at ~30° off-axis, the average effective area for the F4 filter is $\langle A_{\rm eff} \rangle_{(F4)} \sim 300$ cm^2. It can be parametrized as a function of the off-axis angle θ, in the range $\in [0 \div \theta_M]$, as

$$\langle A_{\rm eff}(\theta) \rangle_{(F4)} = A_0 \left[1 - \left(\frac{\theta}{\theta_M} \right)^{\alpha_1} \right]^{\alpha_2} \tag{1}$$

where $A_0 = 366$ cm^2, $\theta_M = 64°$, $\alpha_1 = 3$, and $\alpha_2 = 2$.

Both AGILE PSF and effective area are characterized by a very good off-axis performance and are calibrated well up to almost 60°, showing very smooth variations with the angle relative to the instrument axis.

3. AGILE diffuse gamma-ray model

In the data analysis we use the AGILE diffuse emission model (Giuliani et al. 2004, 2009a) for diffuse γ-ray background-count predictions. Diffuse γ-ray emission includes a combination of two components: (1) diffuse emission from the Galactic interstellar medium and (2) an approximately isotropic extragalactic component, as well as possible contributions from unresolved and faint point sources. Diffuse emission coming from the Galactic plane dominates other components and, as in the EGRET model (Hunter et al. 1997), it is assumed to be produced by the interaction of cosmic rays with the interstellar medium through three physical processes: proton-proton collision, Bremsstrahlung, and inverse Compton emission.

The AGILE diffuse emission model substantially improves the previous EGRET model by using state-of-the-art neutral hydrogen (HI) and CO updated maps to model the matter distribution in the Galaxy. It is based on a 3-D grid with 0.25×0.25 square degrees binning in Galactic longitude and latitude, and a

0.2 kpc step in distance along the line of sight. For the distribution of neutral hydrogen, we used the Leiden-Argentine-Bonn (LAB) Survey of Galactic HI (Kalberla et al. 2005). The LAB survey improves previous results especially in terms of sensitivity (by an order of magnitude), velocity range, and resolution. To properly project the velocity-resolved radio data, we used the Galactic rotation curves parameterized by Clemens et al. (1985). The detailed and relatively high-resolution distribution of molecular hydrogen is obtained from the CO observations described in Dame et al. (2001). The CO is assumed to be a tracer of molecular hydrogen, through a known ratio between hydrogen density and CO radio emissivity. Cosmic rays can emit γ-rays through the inverse Compton mechanism due to their interaction with photons of the cosmological background and of the interstellar radiation field (ISRF). To account for this component, we used the analytical model proposed by Chi & Wolfendale (1991). It describes the ISRF as the result of three main contributions: far infrared (due to dust emission), near infrared, and optical/UV (due to stellar emission). The distribution of cosmic rays (both protons and electrons) in the Galaxy was obtained using the GALPROP cosmic-ray model (Strong et al. 2004; Moskalenko et al. 2007).

4. AGILE data flow and Cycle-1 observational program

AGILE satellite raw Telemetry data are down-linked approximately every 100 min to the ASI Malindi ground station in Kenya and transmitted first to the Mission Control Center at Telespazio, Fucino, and subsequently to the AGILE Data Center (ADC) for data reduction, scientific processing, and archiving. The ADC is the scientific component of the AGILE ground segment and is part of the ASI Science Data Center (ASDC) located in Frascati (Italy). The ADC includes scientific personnel from both the ASDC and the AGILE Team. More details on the ADC organization and tasks will be given in Pittori et al. (2009).

The AGILE pointings are subject to strict constraints requiring that the fixed solar panels always be oriented within 3° from the Sun direction. AGILE pointings are called Observation Blocks (OBs) and usually consist of predefined long exposures, typically lasting 10–30 days, drifting about 1 degree per day with respect to the initial boresight direction to match solar panels illumination constraints. The large GRID FoV (~2.5 sr) and the low altitude orbit imply that, for most pointing directions, the Earth (partially) occults the FoV, thus the observing efficiency and exposure for a given source varies depending on its coordinates. To eliminate the Earth-albedo γ-ray contamination originating from interactions of cosmic rays with the upper atmosphere, a limb-angle cut was applied for all the γ-ray events with reconstructed directions less than 80° with respect to the satellite-Earth vector. With this event selection we do not expect systematic effects caused by albedo photon-background fluctuations.

A predefined AGILE baseline pointing plan, aimed at reaching specific scientific goals that maximize the scientific output of the mission, is made public in advance at the AGILE web pages at ASDC[1] to allow for the organization of multi-wavelength campaigns. Part of the AGILE science program is open to guest observers on a competitive basis through Announcements of Opportunity. Guest observers can apply for data which will be collected within the pointing plan. In case of Target of Opportunity (ToO) observations, the baseline plan is interrupted
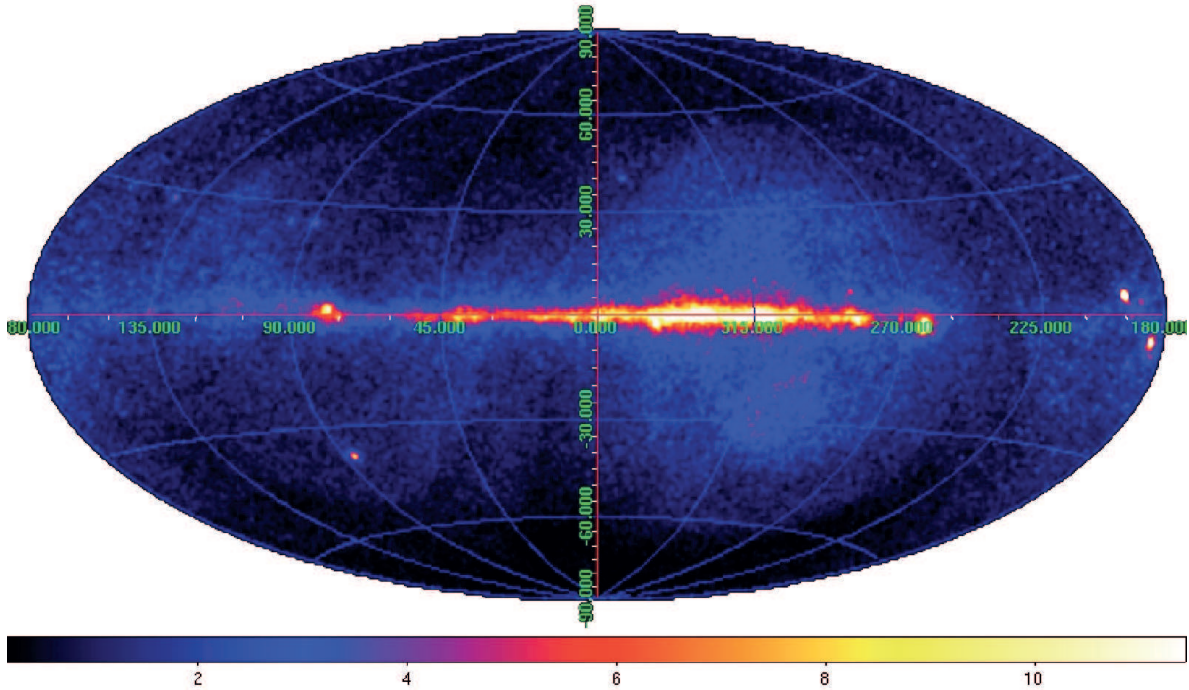
---

[1] http://agile.asdc.asi.it

Fig. 2. Total AGILE-GRID count map in Aitoff projection and Galactic coordinates, for energies >100 MeV in units of ph cm^{-2} s^{-1} sr^{-1} accumulated during the period July 9, 2007–June 30, 2008 (with the F4 event filter). The effect of the nonuniform exposure is particularly evident for pointings centered near the Carina-Crux region.

and resumed at the end of the ToO, so that usually a ToO replaces some of the foreseen baseline pointings, and does not shift in time the execution of the remaining planned observations. The ADC web pages provide interactive tables for both the predefined AGILE baseline pointing plan and the actual list of pointings, including previously unforeseen ToOs.

In this paper we analyzed AGILE-GRID data of the 63 Observation Blocks reported in Table 2, covering the period from July 9, 2007 to June 30, 2008. The total γ-ray exposure and counts maps obtained over the selected period with the F4 filter, in Aitoff projection and Galactic coordinates, are shown in Figs. 1 and 2, respectively.

5. AGILE data reduction and analysis

Raw AGILE telemetry received at ADC is archived and transformed in FITS format through the AGILE Pre-Processing System (TMPPS) (Trifoglio et al. 2008). All GRID data are then routinely processed using the scientific data reduction software tasks developed by the AGILE instrument team and integrated into an automatic pipeline system developed at the ASI Science Data Center. The first step of the pipeline converts the satellite data time into terrestrial time (TT) on a contact-by-contact basis, and performs some preliminary calculations and unit conversions. A second step consists of the γ-ray event selection. We use an AGILE-GRID specific implementation of the Kalman Filter technique for track identification, event direction, and energy reconstruction (Giuliani et al. 2006; Pittori & Tavani 2002). A quality flag is assigned to each event depending on whether it is recognized as a γ-ray event, a charged particle, a "single-track" event, or an event of uncertain classification. An AGILE auxiliary (LOG) file is created, containing all the spacecraft information relevant to the computation of the effective exposure and livetime. Finally, the event directions in sky coordinates are reconstructed and reported in the AGILE event files (EVT),

excluding events flagged as charged background particles. This step produces the Level-2 archive of LOG and EVT files on temporal intervals of few hours. A third step in the pipeline creates quick look (QL) counts, exposure, and diffuse γ-ray emission maps on different timescales: days, weeks, and daily increments on the OB timescale.

At the completion of each OB, we run the AGILE standard analysis OB pipeline that removes the data corresponding to re-pointing slews and occasional losses of fine-pointing attitude. GRID data used in our analysis have been processed with the standard software and in-flight calibrations available at the time of writing[2]. We used the high-quality F4 event filter[3], whose response characteristics were described in Sect. 2.

The standardized and cleaned OB Level-2 archive is the basis for creating guest observers data packets and for the data merging used to build this first catalog.

5.1. Data merging from the OB archive

To merge the data from different observing periods over the whole sky, we produced sets of FITS images in the ARC projection (Calabretta & Greisen 2002) in Galactic coordinates, with a radius of 40° and a bin size of 0.25° × 0.25°, oriented with the north Galactic pole facing upward. The centers of the maps were chosen according to the HEALPix (Hierarchical Equal Area isoLatitude Pixelization) algorithm (Górski et al. 2005) with $N_{side} = 4$, for the coverage of the full sky with 192 maps, whose centers are at a constant latitude. The HEALPix algorithm produces a subdivision of a spherical surface in which each pixel covers the same surface area as every other pixel. However, the

---

[2] Software build version: BUILD GRID_STD_16 and BUILD GRID_SCI_15.2.

[3] New filter algorithms highly efficient and optimized over a wider FoV have been developed and will be distributed by ADC during Cycle-2.

HEALPix projection in FITS (Calabretta & Roukema 2007) is not used here. Only the property of the HEALPix grid that the pixel centers occur on a discrete number of rings of constant latitude is used to represent all-sky γ-ray data binned in sky coordinates. The circular sky areas defined by a centroid and a radius constructed around the 192 HEALPix points are hereafter called "rings".

For each 12-h period, we produced maps of counts and exposure in the full energy band $E = 100$ MeV–50 GeV in rings yielding at least 20 min of effective exposure time within 30° from each HEALPix point[4]. The 12-h maps covering the whole sky were then summed over the entire one-year data span and analyzed with two independent source detection algorithms as described in the next section.

5.2. Source detection method

The AGILE source detection method is based on a maximum likelihood (ML) analysis to derive the best parameter estimates of source significance, γ-ray flux, and source location for each candidate source (Chen et al. 2009). The ML statistical technique, already used in the past in the analysis of γ-ray data (Mattox et al. 1996), compares measured counts in each pixel with the predicted counts derived from the diffuse γ-ray model to find statistically significant excesses consistent with the instrument point spread function. In the analysis we use the AGILE diffuse γ-ray model described in Sect. 3 for diffuse background (gas) map generation.

The likelihood ratio test is then used to compare the null (diffuse background-only) hypothesis with the possible presence of point-source components. According to Wilks' theorem (Wilks 1938), the point source "test statistic" (TS), defined as

$$TS = -2\,(\ln L_0 - \ln L_1) \qquad (2)$$

is expected to behave as χ_1^2 in the null hypothesis, plus terms of order $O(N^{-1/2})$, where N is the number of counts. In practice for a number of AGILE counts $N > 20$, the significance of a source detection at a certain position is given by a number of standard deviations σ equal to $\sqrt{TS}$.

Our method for source detection consists of three steps:

1) preliminary automatic detection of counts map excesses and ML analysis on the resulting fixed positions. This step was performed with two independent detection strategies (A and B described below);
2) selection of high-confidence detections, according to the criteria described below;
3) refined analysis with a ML multi-source task to optimize source locations and flux estimates.

In step 1) two independent automatic source detection strategies over each ring count map were used:

A) identification of possible source locations using the standard Ximage[5] software for astronomical imaging (Giommi et al. 1992), adapted to γ-ray data analysis, and then single source

ML analysis (with the *AG_srctest_fixed* task of the AGILE scientific pipeline). The Ximage detection algorithm locates point sources using a sliding-cell method so that positions and fluxes of each detected source are evaluated in a box maximizing the signal-to-noise ratio;
B) identification of possible source locations using a dedicated algorithm developed by the AGILE Team called SPOT based on a wavelet filtering technique adapted to γ-ray data (Bulgarelli et al. 2008), followed by a multi-source ML analysis (with the task *AG_srclist*) used iteratively.

The AGILE SPOT algorithm used as method B) is a two-step procedure that extracts the excesses from counts maps and builds a list of candidate gamma-ray objects that are then analyzed by a likelihood method. To determine count excesses over the background, the SPOT algorithm analyzes the binned count maps with a smoothing of 1 degree, considers the bins with the largest number of counts, and adds to them the neighboring bins, thereby increasing the connected region, as described in (Di Stefano & Bulgarelli 1999). The process ends when another connected region is merged with the first growing region. At that point, the merging step is reversed and two distinct connected regions are obtained. The centroids of all regions obtained in this way identify the positions of the gamma-ray candidate sources to be analyzed by a multi-source ML. Method A), which uses a single source likelihood analysis, typically optimizes detections of isolated γ-ray sources in extragalactic sky regions, whereas method B) is more efficient in complex regions such as on the Galactic plane, where multiple source contributions may contaminate the result. In both cases we use an analysis radius of 10° and a single power-law source model with spectral photon index α. In our analysis we adopted a standard value of $\alpha = -2.1$, except for the Vela ($\alpha_{\text{Vela}} = -1.69$) and Geminga ($\alpha_{\text{Gem}} = -1.66$) pulsars. This assumption is motivated by the known Crab-like spectral properties of the majority of EGRET sources and by the relatively small statistical significance of several AGILE sources, limiting our spectral analysis capability with chosen data sample. We postpone a detailed spectral analysis of the sources appearing in this catalog to forthcoming publications.

We populate two databases with all the results obtained with the automatic methods A) and B), and in step 2) we cross-correlate the two subsamples extracted from the database with the following conditions:

– distance of the candidate source location from the center of the ring field of view has to be less than or equal to 30°, in order to perform the 10° data analysis within the confidence region of the chosen F4 filter algorithm (≤40°).
– in each database we create a subsample by associating all the detections within a radius of 90′ to a single entry;
– for sources appearing in different ring areas, we select only detections with minimal distance from the center of the ring FoV;
– we select detections with $\sqrt{(TS)} > 4$, which corresponds to a statistical significance of about 4σ.

We obtain

– 81 source candidates with source detection method A);
– 77 source candidates with source detection method B).

An initial cross-correlation radius of 90′ between the two dataset was used to select high-confidence galactic and extragalactic source candidates.

---

[4] We describe here our choice of parameters for map generation. To reduce the particle background contamination, only events tagged as confirmed γ-ray events were selected (filtercode = 5). The South Atlantic Anomaly data were excluded (phasecode = 18) and all the γ-ray events whose reconstructed directions with respect to the satellite-Earth vector is smaller than 80° (albrad = 80) were also rejected, to eliminate the Earth albedo contamination.

[5] Ximage (Giommi et al. 1992) is part of the NASA's Heasarc Xanadu standard software package for multi-mission X-ray astronomy.
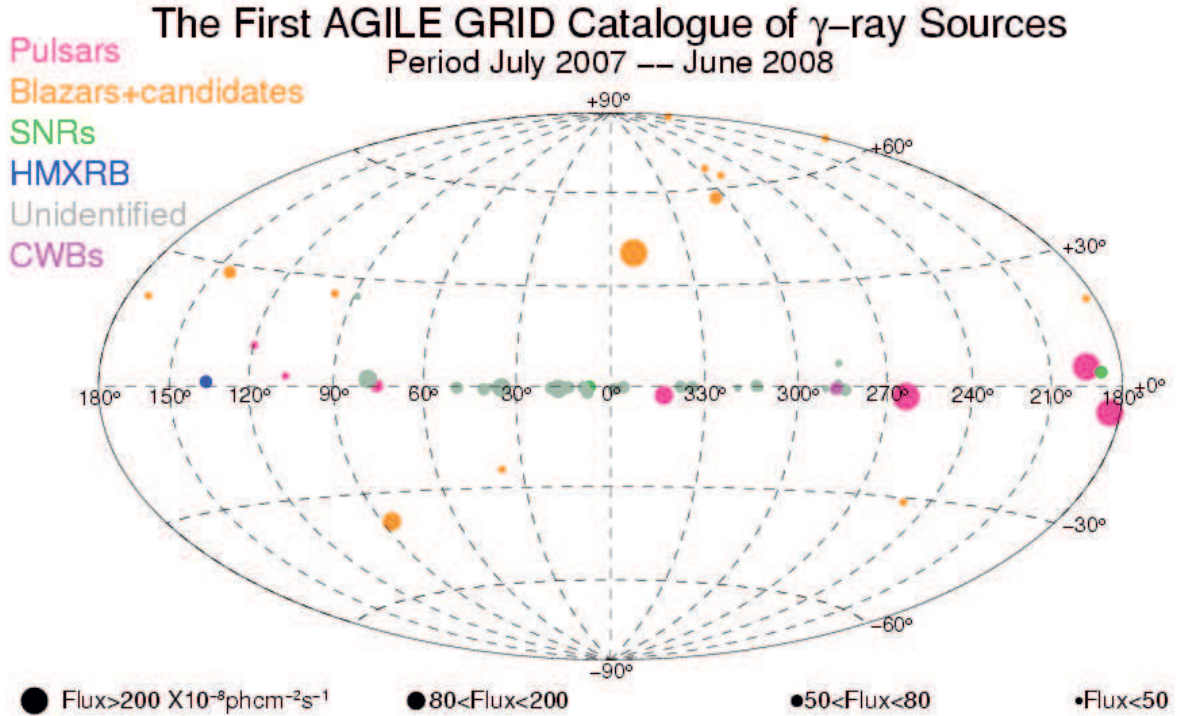
Fig. 3. The First AGILE-GRID Catalog of high-confidence sources, plotted in in Aitoff projection and galactic sky coordinates. Symbol sizes are proportional to source flux values, and symbol colors indicate different source classes.

Then in step 3), a manual refined analysis was performed with a multi-source likelihood analysis task, *AG_multi*, to confirm the detection and derive optimized source parameters. Special care should be used in particular on the galactic plane region ($|b| < 10°$) to deal with possible source confusion and flux contamination. In the analysis of complex regions, positioning results obtained with detection methods A) and B) were also compared with a third standard peak detection software, SExtractor (Bertin & Arnauts 1996), adapted to γ-ray data, using a wavelet filtering and deblending algorithm. We define "high-confidence" as those detections that pass all the requirements described in this section.

6. First AGILE catalog of high-confidence gamma-ray sources

The resulting list of validated sources, detected by using AGILE-GRID data from July 9, 2007 to June 30, 2008 with the method and criteria described in Sect. 5, includes 47 high-confidence sources. The sources of this first AGILE catalog are plotted in Fig. 3 in galactic sky coordinates, classified in Table 1, including both confirmed and possible associations, and listed in Table 3.

In Table 1, for "confirmed" counterparts is meant γ-ray sources for which there are peer-reviewed publications demonstrating high-confidence association with refined analysis methods. Associations for uncertain sources were selected using cross-correlations with various updated public catalogs of γ, hard X-ray, and radio sources either specific mission or specific source classes, such as:

– the Third EGRET catalog (3EG) (Hartman et al. 1999) and the EGRET revised catalog of gamma-ray sources (Casandjian & Grenier 2009);
– the INTEGRAL reference catalog (INTREFCAT) (Ebisawa et al. 2003);

Table 1. Census of the 47 First AGILE high-confidence gamma-ray sources.

Classification	Confirmed counterparts	Possible counterparts
Pulsar	7	14
Blazar FSRQ type	4	3
Blazar BL Lac type	4	–
Blazar Unknown type	–	2
CWB	1	–
SNR	2	–
HMXRB	1	1
Unidentified	–	8

– a selection from the Australian Telescope National Facility (ATNF) pulsar catalog (Manchester et al. 2003);
– HESS source catalog (available on-line);
– the SNR catalog (Green 1991; 2009);
– the Blazar Roma-BZCAT (Massaro et al. 2008).

Summing up, the first AGILE catalog includes 21 confirmed or candidate pulsars, 13 blazars (7 FSRQ, 4 BL Lacs, 2 unknown type), 2 HMXRBs, 2 SNRs, 1 colliding-wind binary system (CWB), and 8 unidentified sources.

In Table 3 we report the values of the following relevant source parameters:

– AGILE source name;
– source position both in celestial and galactic sky coordinates: RA, Dec (J2000), and LII, BII;
– position error (95%), defined as the 2-D error circle radius at 95% confidence level, statistical error only[6];
– the $\sqrt{TS}$ values of the significance of the detection as determined from the refined ML analysis;

---

[6] The AGILE Team recommends adding a systematic error of ±0.1° linearly to this value.

Table 2. AGILE pointings in the period 9 July 2007–30 June 2008, corresponding to the 63 Observation Blocks (OB) considered in our analysis. Acronyms used in table are: ToO = Target of Opportunity pointing, SA = SuperAGILE special pointing.

Region name	OB number	Starting RA, Dec J2000 (deg)	Starting LII, BII (deg)	Start observation (UTC)	End observation(UTC)
3C 279 Region	OB900	195.596, –6.649	307.8118, 56.1183	2007-07-09 12:00	2007-07-13 12:00
VELA Region	OB1000	157.979, –60.214	286.4188, –1.8951	2007-07-13 12:00	2007-07-24 12:00
ToO 3C 454.3	OB1100	17.829, 36.694	127.3645, –26.0059	2007-07-24 12:00	2007-07-30 12:00
ToO 3C 454.3	OB1150	17.829, 36.694	127.3645, –26.0059	2007-07-24 12:00	2007-07-30 12:00
VELA Region	OB1200	150.836, –70.19	289.5293, –11.8265	2007-07-30 12:00	2007-08-01 12:00
SA Crab –45	OB1300	37.097, 12.712	156.5885, –43.7329	2007-08-01 12:00	2007-08-02 12:00
VELA Region	OB1400	176.006, –66.063	296.1593, –4.0824	2007-08-02 12:00	2007-08-12 12:00
SA Crab –35	OB1500	47.41, 16.075	164.8343, –35.3162	2007-08-12 12:00	2007-08-13 12:00
VELA Region	OB1600	195.551, –66.564	304.0044, –3.7154	2007-08-13 12:00	2007-08-22 12:00
SA Crab –25	OB1700	57.139, 18.566	171.0790, –27.3115	2007-08-22 12:00	2007-08-23 12:00
VELA Region	OB1800	216.979, –64.437	313.1071, –3.4890	2007-08-23 12:00	2007-08-27 12:00
Galactic Plane	OB1900	236.570, –41.874	334.4369, 10.0581	2007-08-27 12:00	2007-09-01 12:00
SA Crab (15, 15)	OB2000	69.483, 5.592	190.8962, –26.2858	2007-09-01 12:00	2007-09-02 12:00
SA Crab (0, 15)	OB2100	68.205, 20.566	177.1349, –18.2781	2007-09-02 12:00	2007-09-03 12:00
SA Crab (–15, 15)	OB2200	66.651, 35.559	164.6334, –9.3529	2007-09-03 12:00	2007-09-04 12:00
Field 8	OB2300	51.408, 71.022	134.8816, 11.8210	2007-09-04 12:00	2007-09-12 12:00
SA Crab (0, 5)	OB2400	78.535, 21.730	182.1630, –9.8874	2007-09-12 12:00	2007-09-13 12:00
Field 8	OB2500	74.882, 58.334	150.9906, 9.7255	2007-09-13 12:00	2007-09-15 12:00
SA Crab (45, 0)	OB2600	84.212, –23.014	226.7035, –26.1161	2007-09-15 12:00	2007-09-16 12:00
SA Crab (5, 0)	OB2700	82.987, 16.983	188.5217, –8.9833	2007-09-16 12:00	2007-09-17 12:00
SA Crab (0, 0)	OB2800	83.774, 22.026	184.6179, –5.6675	2007-09-17 12:00	2007-09-18 12:00
SA Crab (–5, 0)	OB2900	84.62, 27.048	180.7737, –2.3343	2007-09-18 12:00	2007-09-19 12:00
SA Crab (–15, 0)	OB3000	85.347, 37.089	172.5873, 3.5179	2007-09-19 12:00	2007-09-20 12:00
SA Crab (–25, 0)	OB3100	86.174, 47.118	164.2603, 9.2213	2007-09-20 12:00	2007-09-21 12:00
SA Crab (–35, 0)	OB3200	87.140, 57.126	155.6110, 14.6016	2007-09-21 12:00	2007-09-22 12:00
SA Crab (–45, 0)	OB3300	88.348, 67.136	146.4473, 19.4825	2007-09-22 12:00	2007-09-23 12:00
SA Crab (0, –5)	OB3400	90.097, 22.143	187.5419, –0.5862	2007-09-23 12:00	2007-09-24 12:00
SA Crab (15, 0)	OB3500	91.034, 7.141	201.1056, –7.1395	2007-09-24 12:00	2007-09-25 12:00
SA Crab (25, 0)	OB3600	91.838, –2.882	210.4602, –11.1195	2007-09-25 12:00	2007-09-26 12:00
SA Crab (35, 0)	OB3700	92.502, –12.926	220.0176, –14.9489	2007-09-26 12:00	2007-09-27 12:00
Crab Nebula	OB3800	94.323, 22.050	189.5211, 2.7938	2007-09-27 12:00	2007-10-01 12:00
SA Crab (0, –15)	OB3900	98.552, 21.875	191.4932, 6.1922	2007-10-01 12:00	2007-10-02 12:00
SA Crab (–15, –15)	OB4000	100.839, 36.784	178.6417, 14.3544	2007-10-02 12:00	2007-10-03 12:00
SA Crab (15, –15)	OB4100	99.566, 6.788	205.3927, 0.1791	2007-10-03 12:00	2007-10-04 12:00
Crab Field	OB4200	101.724, 21.699	192.9681, 8.7550	2007-10-04 12:00	2007-10-12 12:00
SA Crab (0, –25)	OB4300	110.131, 20.718	197.2281, 15.4667	2007-10-12 12:00	2007-10-13 12:00
Gal. Center	OB4400	290.920, –18.896	19.2683, –15.4110	2007-10-13 12:00	2007-10-22 12:00
SA Crab (0, –35)	OB4500	120.494, 18.879	203.0392, 23.7444	2007-10-22 12:00	2007-10-23 12:00
Gal. Center Reg.	OB4600	301.173, –17.107	25.0972, –23.6663	2007-10-23 12:00	2007-10-24 08:00
ToO 0716+714	OB4610	148.939, 67.888	143.3642, 41.5875	2007-10-24 08:00	2007-10-29 12:00
ToO Extended	OB4630	157.461, 66.942	141.5537, 44.7248	2007-10-29 12:00	2007-11-01 12:00
SA Crab (0, –45)	OB4700	130.614, 16.339	209.7914, 31.7351	2007-11-01 12:00	2007-11-02 12:00
Cygnus Region	OB4800	296.880, 34.501	69.5937, 4.6227	2007-11-02 12:00	2007-12-01 12:00
Cygnus Field 1	OB4900	304.432, 53.552	88.8156, 9.9272	2007-12-01 12:00	2007-12-05 09:00
Cygnus Repointing	OB4910	322.496, 38.244	85.1187, –9.4171	2007-12-05 09:00	2007-12-16 12:00
Cygnus Repointing	OB4920	322.496, 38.244	85.1187, –9.4171	2007-12-05 09:00	2007-12-16 12:00
Virgo Field	OB5010	173.433, –0.437	265.6464, 56.7005	2007-12-16 12:00	2008-01-08 12:00
Vela Field	OB5100	147.060, –62.517	283.4703, –6.7881	2008-01-08 12:00	2008-02-01 12:00
South Gal Pole	OB5200	58.347, –37.795	240.3889, –50.5780	2008-02-01 12:00	2008-02-09 09:00
ToO MKN 421	OB5210	250.974, 50.293	77.3096, 40.6278	2008-02-09 09:00	2008-02-12 12:00
South Gal Pole Repointing	OB5220	65.660, –35.714	237.5007, –44.6737	2008-02-12 12:00	2008-02-14 12:00
Musca Field	OB5300	191.934, –71.893	302.6408, –9.0241	2008-02-14 12:00	2008-03-01 12:00
Gal. Center 1	OB5400	243.596, –50.979	332.1063, 0.0207	2008-03-01 12:00	2008-03-16 12:00
Gal. Center 2	OB5450	265.781, –28.626	359.9782, 0.6280	2008-03-16 12:00	2008-03-30 12:00
Anti-Center 1	OB5500	100.944, 21.711	192.6369, 8.1084	2008-03-30 12:00	2008-04-05 12:00
SA Crab (8, 24)	OB5510	108.283, 28.625	188.9607, 16.9953	2008-04-05 12:00	2008-04-07 12:00
SA Crab (15, 26)	OB5520	111.762, 35.688	183.0072, 22.2023	2008-04-07 12:00	2008-04-08 12:00
Anti-Center 2	OB5530	110.404, 20.758	197.2962, 15.7167	2008-04-08 12:00	2008-04-10 12:00
Vulpecula Field	OB5600	286.259, 20.819	53.0394, 6.4733	2008-04-10 12:00	2008-04-30 12:00
North Gal Pole	OB5700	250.075, 72.497	104.8522, 35.4379	2008-04-30 12:00	2008-05-10 12:00
Cygnus Field 2	OB5800	304.286, 35.974	74.0497, 0.2720	2008-05-10 12:00	2008-06-09 18:00
ToO WComae ON+231	OB5810	182.285, 29.614	195.5016, 80.3738	2008-06-09 18:00	2008-06-15 12:00
Cygnus Repointing	OB5820	323.248, 50.079	93.6645, –1.1664	2008-06-15 12:00	2008-06-30 12:00

Table 3. First AGILE high-confidence gamma-ray sources list.

AGILE name	RA (J2000.0) (hh mm ss)	Dec (J2000.0) (dd mm ss)	LII (deg)	BII (deg)	[a]Pos. Error (95%) (deg)	sqrt(TS)	[b]Mean Ring Exp ($\times 10^8$ cm^2 s)	[c]Mean flux & Error ($\times 10^{-8}$ ph cm^{-2} s^{-1})	Classification	Confirmed Counterp.	Possible Counterp. & Other names
1AGL J0006+7311	00 06 34.2	+73 11 06.6	119.65	10.6	0.63	5.1	3.01	23 ± 5	GammaPulsar*	CTA1	3EGJ0010+7309
1AGL J0242+6111	02 42 13.6	+61 11 06.7	135.88	1.13	0.64	5.3	1.17	54 ± 12	HMXRB	LSI+61303	3EGJ0241+6103
1AGL J0535+2205	05 35 05.9	+22 05 41.7	184.56	–5.63	0.09	47.2	2.79	220 ± 15	Pulsar	Crab	3EGJ0534+2200
1AGL J0538-4424	05 38 29.6	–44 24 17.8	250.44	–31.2	0.5	5.9	0.81	43 ± 10	Blazar-BLLac	PKS0537-441	3EGJ0540-4402 BZBJ0538-4405
1AGL J0617+2236	06 17 21.7	+22 36 14.2	189.04	3.07	0.27	9.9	2.79	69 ± 9	SNR	IC443	3EGJ0617+2238
1AGL J0634+1748	06 34 15.8	+17 48 27.7	195.14	4.36	0.05	63	2.79	320 ± 10	Pulsar	Geminga	3EGJ0633+1751
1AGL J0657+4554	06 57 29.2	+45 54 14.5	170.73	20.11	0.55	5.8	1.98	31 ± 6	Blazar	—	BZUJ0654+4514 S40650+45
1AGL J0714+3340	07 14 29.4	+33 40 37.3	184.12	19.1	0.85	4.2	2.57	18 ± 5	Blazar	—	BZUJ0719+3307 GB20716+332
1AGL J0722+7125	07 22 22.9	+71 25 31.1	143.89	28.06	0.37	10.9	1.39	68 ± 9	Blazar-BLLac	S50716+714	3EGJ0721+7120 BZBJ0721+7120
1AGL J0835-4509	08 35 13.3	–45 09 09.0	263.52	–2.79	0.09	41.7	0.81	780 ± 32	Pulsar	VelaPSR	3EGJ0834-4511
1AGL J1022-5822	10 22 08.8	–58 22 17.0	284.39	–0.98	0.36	10.1	4.85	59 ± 7	Unclassified	(C)	3EGJ1013-5915 PSRJ1016-5857
1AGL J1044-5936	10 43 57.6	–59 36 41.3	287.44	–0.63	0.58	5.3	4.85	27 ± 6	CWB	—	EtaCar
1AGL J1043-5749	10 43 56.0	–57 49 51.0	286.60	0.94	0.68	4.5	4.85	22 ± 5	Unclassified	(C)	3EGJ1048-5840
1AGL J1058-5239	10 58 31.1	–52 39 47.5	286.15	6.49	0.30	8.7	4.85	29 ± 4	Unclassified	—	3EG J1058-5234 PSRJ1057-5226
1AGL J1104+3754	11 04 38.5	+37 54 33.6	180.48	65.16	0.66	4.7	0.51	42 ± 13	Blazar-BLLac	Mkn421	3EGJ1104+3809 BZBJ1104+3812
1AGL J1108-6103	11 08 43.6	–61 03 54.3	290.83	–0.63	0.57	6.1	4.85	30 ± 6	Unclassified	—	3EGJ1102-6103 PSRJ1119-6127
1AGL J1222+2851	12 22 39.7	+28 51 02.3	196.09	83.42	0.74	4.7	0.50	38 ± 11	Blazar-BLLac	WComae	3EGJ1222+2841 BZBJ1221+2813 ON +231
1AGL J1228+0142	12 28 59.5	+01 42 41.3	290.04	64.02	0.71	4.7	1.98	24 ± 6	Blazar-FSRQ	3C 273	3EGJ1229+0210 BZQJ1229+0203
1AGL J1238+0406	12 38 31.0	+04 06 14.2	294.74	66.77	1.23	4.7	1.98	25 ± 6	Blazar-FSRQ	—	3EGJ1236+0457 BZQJ1239+0443
1AGL J1256-0549	12 56 33.1	–05 49 42.6	305.27	57.02	0.32	10.2	1.98	65 ± 9	Blazar-FSRQ	3C 279	3EGJ1255-0549 BZQJ1256-0547

C. Pittori et al.: First AGILE catalog

Table 3. continued.

AGILE name	RA (J2000.0) (hh mm ss)	Dec (J2000.0) (dd mm ss)	LII (deg)	BII (deg)	[a]Pos. Error (95%) (deg)	sqrt(TS)	[b]Mean Ring Exp (×10^8 cm^2 s)	[c]Mean flux & Error (×10^{-8} ph cm^{-2} s^{-1})	Classification	Confirmed Counterp.	Possible Counterp. & Other names
1AGL J1412-6149	14 12 06.1	–61 49 32.5	312.3	–0.43	0.44	6.3	5.44	43 ± 7	Unclassified	(C)	3EGJ1410-6147 PSRJ1410-6132 G312.4-0.4
1AGL J1419-6055	14 19 51.2	–60 55 11.2	313.47	0.13	0.31	7.5	5.44	52 ± 7	Unclassified	(C)	3EGJ1420-6038 PSRJ1420-6048
1AGL J1506-5859	15 06 01.5	–58 59 13.5	319.52	–0.52	0.48	6.9	5.44	41 ± 7	Unclassified	—	PSRJ1509-5850
1AGL J1511-0908	15 11 38.5	–09 08 12.8	350.97	40.31	0.33	11.2	0.39	220 ± 32	Blazar-FSRQ	PKS1510-089	3EGJ1512-0849 BZQJ1512-0905
1AGL J1624-4946	16 24 26.9	–49 46 51.9	334.09	–0.25	0.58	5.7	2.18	67 ± 13	Unclassified	—	PSRJ1623-4949
1AGL J1639-4702	16 39 05.5	–47 02 28.2	337.75	–0.15	0.53	6.4	2.18	76 ± 13	Unclassified	—	3EGJ1639-4702 PSRJ1637-4642
1AGL J1709-4428	17 09 12.6	–44 28 44.5	343.07	–2.64	0.20	13.8	2.18	120 ± 11	Pulsar	PSRJ1709-4429	3EGJ1710-4439
1AGL J1736-3235	17 36 19.9	–32 35 00.8	355.85	–0.24	0.59	5.1	1.56	69 ± 15	Unclassified	(C)	3EGJ1734-3232
1AGL J1746-3017	17 46 01.5	–30 17 23.7	358.89	–0.78	0.68	4.4	1.56	66 ± 16	Unclassified	(C)	3EGJ1744-3011
1AGL J1801-2317	18 01 22.7	–23 17 20.1	6.66	–0.18	0.35	5.8	1.56	69 ± 13	SNR	W28	3EGJ1800-2338 HESSJ1801-233
1AGL J1806-2143	18 05 39.5	–21 43 21.2	8.51	–0.27	0.75	4.3	1.56	54 ± 13	Unclassified	(C)	PSRJ1803-2137 W30 HESSJ1804-216
1AGL J1809-2333	18 09 22.8	–23 32 56.3	7.33	–1.91	0.35	5.9	1.56	53 ± 10	Unclassified	—	3EGJ1809-2328
1AGL J1815-1732	18 15 29.7	–17 32 27.1	13.29	–0.28	0.65	4.4	1.56	52 ± 13	Unclassified	—	PSRJ1815-1738 HESSJ1813-178
1AGL J1824-1455	18 23 32.5	–14 54 41.3	16.52	–0.74	0.52	7.3	1.56	86 ± 13	Unclassified	(C)	3EGJ1824-1514 G16.410.55 LS 5039
1AGL J1827-1227	18 26 57.8	–12 46 58.6	18.79	–0.48	0.54	6.5	1.56	79 ± 13	Unclassified	—	3EGJ1826-1302 HESSJ1825-137
1AGL J1836+5923	18 36 14.8	+59 23 30.4	88.84	24.99	0.17	15.6	5.52	45 ± 4	Unclassified	—	3EGJ1835+5918 BZBJ1841+5906
1AGL J1846+6714	18 46 19.6	+67 14 17.4	97.59	25.35	0.43	7.0	5.52	20 ± 4	Blazar-FSRQ	—	BZQJ1849+6705 4C66.20
1AGL J1856+0122	18 55 57.7	+01 22 24.5	34.67	–0.38	0.25	11.5	3.90	123 ± 12	Unclassified	—	3EGJ1856+0114 W44 PSRJ1856+0113

Table 3. continued.

AGILE name	RA (J2000.0) (hh mm ss)	Dec (J2000.0) (dd mm ss)	LII (deg)	BII (deg)	[a]Pos. Error (95%) (deg)	sqrt(TS)	[b]Mean Ring Exp ($\times 10^8$ cm^2 s)	[c]Mean flux & Error ($\times 10^{-8}$ ph cm^{-2} s^{-1})	Classification	Confirmed Counterp.	Possible Counterp. & Other names
1AGL J1901+0429	19 01 20.8	+04 29 38.5	38.06	–0.15	0.58	4.4	3.06	45 ± 11	Unclassified	—	PSRJ1901+0435
1AGL J1908+0614	19 08 08.4	+06 14 34.5	40.39	–0.85	0.45	7.7	3.06	76 ± 11	Unclassified	—	3EGJ1903+0550 PSRJ1905+0616
1AGL J1923+1404	19 22 53.7	+14 03 45.2	49.00	–0.42	0.64	6.6	4.00	60 ± 10	Unclassified	(C)	W51 PSRJ1921+1419
1AGL J2021+3652	20 21 25.3	+36 52 32.6	75.28	0.07	0.19	14.2	8.31	65 ± 5	Pulsar	PSRJ2021+3651	3EGJ2021+3716
1AGL J2022+4032	20 22 08.5	+40 32 13.4	78.37	2.04	0.12	23.4	8.31	120 ± 7	Unclassified	—	3EGJ2020+4017 SNR Gamma Cygni
1AGL J2026-0732	20 26 30.7	–07 32 45.3	37.05	–24.55	0.53	6.9	3.06	39 ± 7	Blazar-FSRQ	—	3EGJ2025-0744 BZQJ2025-0735 PKS2023-07
1AGL J2032+4102	20 32 27.7	+41 02 00.0	79.91	0.74	0.41	6.8	8.31	37 ± 6	Unclassified	—	3EGJ033+4118 CygX-3
1AGL J2231+6109	22 31 07.1	+61 09 46.7	106.82	2.76	0.29	8.4	6.26	32 ± 5	Pulsar	PSRJ2229+6114	3EGJ2227+6122
1AGL J2254+1602	22 54 10.3	+16 02 32.6	86.09	–38.3	0.17	23.0	1.16	200 ± 14	Blazar-FSRQ	3C454.3	3EGJ2254+1601 BZQJ2253+1608

[a] 2D error circle radius at 95% confidence level, statistical error only. The AGILE Team recommends adding a systematic error of ±0.1 degrees linearly.

[b] Mean value of the exposure map relative to the sky area (Ring) used for each source analysis.

[c] $E > 100$ MeV flux and its 1σ statistical error. The AGILE Team recommends adding a systematic error of 10% to the statistical error.

- the mean value of the F4 exposure map in units of 10^8 cm^2 s, relative to the sky area (Ring) used for each source analysis;
- the source flux above 100 MeV and its 1σ statistical error[7] in units of 10^{-8} ph cm^{-2} s^{-1}. This is the average source flux value over the entire time period;
- source classification;
- counterpart name for confirmed sources;
- possible counterparts in the AGILE error radius and other names, both for "confirmed" and "uncertain" counterparts.

6.1. Notes on individual sources

As described in Sect. 5, pointlike γ-ray sources parameters reported in this paper are determined by a likelihood analysis of the 10° field surrounding the candidate sources. The analysis depends on the local Galactic diffuse emission, the γ-ray photon statistics, the instrument PSF, the response matrix as a function of energy and off-axis angle, and on the background filtering. Particular care is required to carry out the analysis in regions of the Galactic plane that are characterized by a relatively high and structured flux of the diffuse Galactic emission, as well as in regions harboring nearby γ-ray sources leading to possible source confusion. For such regions we insert the label (C), for "Confused", in the Confirmed Counterpart column of Table 3. These are significant AGILE detections, which however have flux and location parameters that may be affected (within the statistical+systematic errors) by other nearby sources. In the following we briefly comment on some specific AGILE detections.

1AGL J0006+7311. This AGILE source, positionally coincident with the EGRET γ-ray source 3EG J0010+7309 located in supernova remnant CTA 1, is associated with the first radio quiet pulsar recently discovered through its γ-ray pulsations by the Fermi Gamma-Ray Space Telescope (Abdo et al. 2008). This new class of young pulsar sources may be possibly associated with most unidentified Galactic γ-ray sources in star-forming regions and SNRs. Search for pulsations in γ-ray AGILE data is currently under way. At the border of the AGILE error box, there is also the blazar source BZQ J0019+7327.

1AGL J0535+2205 and 1AGL J0634+1748 (Crab and Geminga). These two well known strong γ-ray pulsars, together with the Vela pulsar, were used for in-flight AGILE calibrations. We report the flux values obtained during calibration subperiods. These values agree with pulsed flux values reported in (Pellizzoni et al. 2009). We note, however, that we observed higher flux values, over 1σ from the reported mean flux, for both sources when merging all the data, including shorter (1 day) integration periods during 2007. This point is under investigation.

1AGL J0617+2236. This AGILE detection provides an improved positioning compared to the 3EG J0617+2238 error box. This source is positionally coincident with the SNR IC443 (Tavani et al. 2009c). The AGILE error box also contains the PSR J0614+2229.

1AGL J0657+4554 and 1AGL J0714+3340. These two high-latitude ($|b| > 10$ deg) AGILE sources, associated with blazars

---

[7] The AGILE Team recommends adding a systematic error of 10% to the flux statistical error.

of unknown type in the BZCAT, have no EGRET counterparts probably owing to flux variability.

1AGL J0835-4509 (Vela pulsar). As the most luminous steady source in the γ-ray sky, Vela has been extensively used for in-flight AGILE-GRID calibrations. With the F4 filter version and the strict criteria used to build this first catalog, the resulting effective exposure is quite low (only about 0.81×10^8 cm^2 s on source over the entire period).

1AGL J1022-5822. This source lies in the complex Carina region, and multiple source contributions are possible.

1AGL J1043-5931. This source (not detected by EGRET) is close to 1AGL J1043-5749 in the Carina region. Our refined analysis leads to the association of this γ-ray source with the colliding wind binary Eta Carinae (Tavani et al. 2009d).

1AGL J1104+3754 and 1AGL J1222+2851. The effective exposure on these sources is low, just about 2 effective days, but it includes a ToO period on the source W Comae.

1AGL J1412-6149 and 1AGL J1419-6055. This source lies in the complex Crux region, and multiple source contributions are possible.

1AGL J1511-0908. The total effective exposure on this source is very low, just about 2 effective days, but it includes a ToO period on the associated source PKS 1510-089.

1AGL J1736-3235, 1AGL J1746-3017. These sources are in the complex region around 10° from the Galactic center, and multiple source contributions are possible. We emphasize the relatively small exposure of the Galactic center region achieved until June 30, 2008, which does not allow a deeper analysis of the complex γ-ray emission from the center of our Galaxy.

1AGL J1801-2317. This source is spatially coincident with the TeV source HESS J1801-233. Remarkably, they both appear to be associated with the northeastern section of the SNR W28 shell (Giuliani et al. 2009b).

7. Conclusions

The AGILE Cycle-1 pointing plan covered the whole sky focusing mainly toward the Galactic plane. The AGILE first catalog includes only high-significance sources characterized by a prominent mean γ-ray flux above 100 MeV when integrated over the total exposure period 2007 July–2008 June. With our one-year long integration, only sources with "steady" flux values above $\sim 20 \times 10^{-8}$ ph cm^{-2} s^{-1} are detected over 4σ. Source detections during flaring state and determination of peak fluxes are not included in this catalog. This should be taken into account when comparing with the results of the third EGRET catalog, which includes detections over 4σ in each of the EGRET viewing periods during its effective 6-year lifetime. An analysis of γ-ray detection by the AGILE-GRID on short timescales (several weeks, 1-week, days) is beyond the scope of this catalog, so will be published elsewehere. The AGILE-GRID spatial resolution reached with long exposures is substantially better than that of EGRET, and the total exposure accumulated by AGILE in several sky regions, particularly near the Galactic plane, is comparable to the one obtained by EGRET in 6 years effective time. It is then interesting to compare the relatively high-flux

sources detected by AGILE with the equivalent sources of the third EGRET catalog. Many bright γ-ray sources detected by EGRET are confirmed by AGILE, which provides comparable or better positioning. AGILE in the first catalog detected five sources that were not present in the 3EG catalog: 3 blazars and 2 candidate pulsars. As expected from statistical detection effects and source variability, some of the prominent (with flux range $40-100 \times 10^{-8}$ ph cm^{-2} s^{-1}) 3EG sources in the Galactic plane are not detected by AGILE with mean flux values at a significance level that is sufficient to be included in this first catalog.

It is also important to note that the AGILE-GRID exposure in the selected period has been accumulated mostly in the Carina-Crux and in the Cygnus regions, with relatively low exposure at the Galactic center. This explains the relatively small number of sources in the Galactic center region.

Finally, taking into account that the AGILE first catalog is not a complete flux-limited sample and is affected by selection effects due to the assumed fixed value (-2.1) of the unknown source spectral indices, we observe that with a limiting flux of about 2×10^{-7} ph cm^{-2} s^{-1}, the number and rate of γ-ray Blazars observed by AGILE (13 Blazars: 7 FSRQs and 5 BL Lacs) is roughly consistent with expectations from the EGRET log N–log S (Özel & Thompson 1996; Mücke & Pohl 2000). A detailed study over a complete AGILE AGN sample will be performed in the future.

A variability study of the sources of this first catalog on different timescales will appear in Verrecchia et al. (2009).

References

Abdo, A. A., Ackermann, M., Atwood, W. B., et al. 2008, Science, 322, 1218
Argan, A., et al. 2004, in Science Symposium Conference Record, 375, 371
Atwood, W. B., Abdo, A. A., Ackermann, M., et al. 2009, ApJ, 697, 1071
Barbiellini, G., Bordignon, G., Fedel, G., et al. 2001, AIP Conf. Proc., 587, 754
Bennet, K., Lichti, G. G., Bignami, G. F., et al. 1977, A&A, 56, 469
Bertin, E., & Arnauts, S. 1996, A&AS, 117, 393
Bignami, G. F., Boella, G., Burger, J. J., et al. 1975, Space Sci. Instr., 1, 245
Bulgarelli, A., Trifoglio, M., Gianotti, F., et al. 2008, Proceedings of Astronomical Data Analysis Software and Systems XVIII, Quebec, Canada, ADASS, ASP Conf. Ser.
Calabretta, M. R., & Greisen, E. W. 2002, A&A, 395, 1077
Calabretta, M. R., & Roukema, B. F. 2007, MNRAS, 381, 865
Casandjian, J. M., & Grenier, I. A. 2008, A&A, 489, 849
Chen, A., et al. 2009, in preparation
Chi, X., & Wolfendale, A. W. 1991, J. Phys. G, 17, 987
Clemens, D. P. 1985, ApJ, Part 1, 295, 422
Dame, T. M., Hartmann, D., & Thaddeus, P. 2001, ApJ, 547, 792
Di Stefano, L., & Bulgarelli, A. 1999, Proceedings of the 10th International Conference on Image Analysis and Processing (ICIAP 1999), 322
Ebisawa, K., Bourban, G., Bodaghee, A., Mowlavi, N., & Courvoisier, T. J.-L. 2003, A&A, 411, L59
Feroci, M., Costa, E., Soffitta, P., et al. 2007, NIM A, 581, 728
Fichtel, C. E., et al. 1975, ApJ, 198, 163
Gianotti, F., & Trifoglio, M. 2001, in Astronomical Data Analysis Software and Systems X, ed. F. R. Harnden, Jr., F. A. Primini, & H. E. Payne, ASP Conf. Ser., 238, 245
Giommi, P., Angelini, L., Jacobs, P., & Tagliaferri, G. 1992, Astronomical Data Analysis Software and Systems I, ASP Conf. Ser., 25
Giuliani, A., Chen, A., Mereghetti, S., et al. 2004, Mem. SAIt Suppl., 5, 135
Giuliani, A., Cocco, V., Mereghetti, S., Pittori, C., & Tavani, M. 2006, NIM A, 568, 692
Giuliani, A., et al. 2009a, in preparation
Giuliani, A., et al. 2009b, in preparation
Green, D. A. 1991, PASP, 103, 209
Green, D. A. 2009, Bull. Astron. Soc. India, 37, 45
Górski, K. M., Hivon, E., Banday, A. J., et al. 2005, ApJ, 622, 759
Hartman, R. C., Bertsch, D. L., Bloom, S. D., et al. 1999, ApJS, 123, 79H
Hunter, S. D., Bertsch, D. L., Catelli, J. R., et al. 1997, ApJ, 481, 205
Kalberla, P. M. W., Burton, W. B., Hartmann, D., et al. 2005, A&A, 440, 775
Labanti, C., Marisaldi, M., Fuschino, F., et al. 2006, SPIE, 6266, 62663
Labanti, C., Marisaldi, M., Fuschino, F., et al. 2009, NIM A, 598, 470
Manchester, R. N., Hobbs, A. T., & Hobbs, M. 2005, AJ, 129, 1993
Massaro, E., Giommi, P., Leto, L., et al. 2008 [arXiv:0810.2206], on-line interactive table available at http://www.asdc.asi.it/bzcat
Mattox, J. R., Bertsch, D. L., Chiang, J., et al. 1996, ApJ, 461, 396
Michelson, P. F. 2008, APS Meeting Abstracts, TSSP, L2002
Moskalenko, I. V., Strong, A. W., Digel, S. W., & Porter, T. A. 2007, AIP Conf. Proc., 921, 490
Mücke, A., & Pohl, M. 2000, MNRAS, 312, 177
Özel, M. E., & Thompson, D. J. 1996, AJ, 463, 105
Pellizzoni, A., Pilia, M., Possenti, A., et al. 2009, ApJ, 691, 1618
Perotti, F., Fiorini, M., Incorvaia, S., Mattaini, E., & Sant'Ambrogio, E. 2006, NIM A, 556, 228
Pittori, C., & Tavani, M. 2002, NIM A, 488, 295
Pittori, C., et al. 2009, in preparation
Prest, M., Barbiellini, G., Bordignon, G., et al. 2003, NIM A, 501, 280
Strong, A. W., Moskalenko, I. V., & Reimer, O. 2004, ApJ, 613, 962
Tavani, M., Barbiellini, G., Argan, A., et al. 2008, for the AGILE Collaboration, NIM A, 588, 52 [arXiv:0807.4254]
Tavani, M., Barbiellini, G., Argan, A., et al. 2009a, for the AGILE Collaboration, A&A, 502, 1015
Tavani, M., et al. 2009b, in preparation
Tavani, M., et al. 2009c, in preparation
Tavani, M., Sabatini, S., Pian, E., Bulgarelli, A., et al. 2009d, ApJ, 698, L142
Thompson, D. J., Bertsch, D. L., Fichtel, C. E., et al. 1993, ApJS, 86, 629
Trifoglio, M., Bulgarelli, A., Gianotti, F., et al. 2008, Proc. SPIE, 7011, 70113E
Wilks, S. S. 1938, Ann. Math. Stat., 9, 60